WUSCHEL acts as a rheostat on the auxin pathway to maintain apical stem cells in *Arabidopsis*

Yanfei Ma[1§], Andrej Miotk[1§], Zoran Šutiković[1], Anna Medzihradszky[1], Christian Wenzl[1], Olga Ermakova[1], Christophe Gaillochet[1], Joachim Forner[1], Gözde Utan[1], Klaus Brackmann[3], Carlos S. Galvan-Ampudia[4], Teva Vernoux[4], Thomas Greb[2] & Jan U. Lohmann[1*]

[1]Department of Stem Cell Biology, Centre for Organismal Studies, Heidelberg University; D-69120 Heidelberg, Germany

[2]Department of Developmental Physiology, Centre for Organismal Studies, Heidelberg University; D-69120 Heidelberg, Germany

[3]Gregor Mendel Institute (GMI), Austrian Academy of Sciences, Vienna Biocenter (VBC), Dr. Bohr-Gasse 3, 1030 Vienna, Austria

[4]Laboratoire Reproduction et Développement des Plantes, Univ Lyon, ENS de Lyon, UCB Lyon 1, CNRS, INRA, F-69342 Lyon, France

[§] these authors contributed equally and are listed alphabetically

*corresponding author

Mailing address of corresponding author:

Jan U. Lohmann
Department of Stem Cell Biology
University of Heidelberg
Im Neuenheimer Feld 230
D-69120 Heidelberg
Germany

PH: +49 6221 546269
FX: +49 6221 546424
EM: jlohmann@meristemania.org

Abstract

During development and growth, dynamic signals need to be translated into spatially precise and temporally stable gene expression states, which define cell fate. In the context of the apical plant stem cell system, local accumulation of the small, highly mobile phytohormone auxin triggers organ initiation. Here, we show that the WUSCHEL transcription factor locally protects stem cells from differentiation by controlling the auxin signaling and response pathway via regulation of histone acetylation. Conversely, low levels of signaling are required for stem cell maintenance, demonstrating that WUSCHEL acts as a rheostat on the auxin pathway. Our results reveal an important mechanism that allows cells to differentially translate a potent and highly mobile developmental signal into appropriate cell behavior with high spatial precision and temporal robustness.

Main Text

The shoot apical meristem (SAM) is a highly dynamic and continuously active stem cell system responsible for the generation of all above ground tissues of plants. The stem cells are located in the central zone and are maintained by a feedback loop consisting of the stem cell promoting WUSCHEL (WUS) homeodomain transcription factor and the restrictive CLAVATA (CLV) pathway[1,2]. WUS protein is produced by a group of niche cells, called organizing center, and moves to stem cells via plasmodesmata[3,4]. Stem cells are surrounded by transient amplifying cells, which are competent to undergo differentiation in response to auxin, a small, mobile signaling molecule with diverse and context specific roles in plant development and physiology (reviewed in ref. 5). Auxin sensing is dependent on nuclear receptors, whose activation triggers the proteolytic degradation of AUX/IAA proteins, such as BODENLOS (BDL), which inhibit the function of activating AUXIN RESPONSE FACTOR (ARF) transcription factors[6-8]. Intracellular accumulation of auxin is regulated by active polar transport and in the context of the SAM, the export carrier PINFORMED1 (PIN1) determines the sites of lateral organ initiation and thus differentiation[9,10]. Here we ask how long-term stem cell fate is robustly maintained within such a highly dynamic signaling system geared towards differentiation.

Results

Role of auxin signaling for apical stem cell fate

As a first step, we mapped auxin signaling behavior using the genetically encoded markers R2D2 and DR5v2 (ref. 11). R2D2 is based on fusing the auxin-dependent degradation domain II of an Aux/IAA protein to Venus fluorescent protein, and uses a mutated, non-degradable domain II linked to tdTomato as an internal control[11]. Hence, R2D2 signal is dictated by the levels of auxin as well as the endogenous receptors and represents a proxy for the auxin signaling input for every cell. Computational analysis of the green to red ratio in plants carrying R2D2 demonstrated that auxin is present and sensed fairly uniformly across the SAM including the central stem cell domain, with local minima only detected at organ boundaries (Fig. 1a, b and refs. 12,13). In contrast, DR5v2, a reporter for auxin signaling output based on a synthetic promoter containing repeats of ARF DNA binding sites[11], was strongly activated non-uniformly in wedge shaped zones of differentiation competent cells, but only weakly expressed the center of the SAM (Fig. 1d; and ref. 12). Leveraging the sensitivity of DR5v2 and the expression of the *CLV3* stem cell

marker in the same transgenic line, we observed that the auxin response minimum invariantly coincided with a small group of cells in the stem cell domain (Fig. 1c-f).

To test if the auxin output minimum is functionally connected to stem cell identity, we interfered with their maintenance. To this end, we induced symplastic isolation through callose deposition at plasmodesmata of stem cells, which we had shown earlier to induce their differentiation[4,14]. Following auxin signaling output over time, we observed activation of DR5v2 in the central zone domain after 36 hours of callose synthase (iCalSm) expression and cell expansion, a hallmark of plant cell differentiation, after 72 hours (Fig. 2a-e; Extended Fig. 1-3; Extended Table 1). Thus, stem cell fate and the auxin response minimum appeared to be functionally connected, leading us to hypothesize that manipulation of auxin signaling in the central zone should affect stem cell behavior. To test this directly we designed a transgene, which allowed us to suppress auxin signaling output specifically in stem cells by fusing the dominant auxin signaling output inhibitor *BDL-D* with the glucocorticoid receptor tag. The activity of the resulting fusion protein could be induced by dexamethasone (DEX) treatment, which facilitated the translocation of BDL-D-GR into the nucleus[15]. In line with our expectations, we found that inducing *pCLV3:BDL-D-GR* led to an expansion of the DR5v2 minimum in the center of the SAM (Fig. 2 f, g). Surprisingly, long term induction of BDL-D-GR or stem cell specific expression of *BDL-D* caused meristem termination in half of the seedlings (n=90; Fig. 2 k, l), demonstrating that stem cells require active auxin signaling for their maintenance. In contrast, expression of a potent positive signaling component, the auxin response factor *ARF5/MONOPTEROS (MP),* or its constitutively active form *MPΔ,* which engages the auxin pathway independently of signal perception[16], did not cause relevant reduction in meristem size (Fig. 2 h-j, o and ref. 17). When expressed throughout the entire SAM, *MPΔ* stimulated ectopic organ initiation specifically in the peripheral zone (Fig. 2n; Extended Fig. 4), demonstrating that resistance to auxin was not a general feature of the meristem, but limited to stem cells. Importantly, the DR5v2 reporter, which senses auxin output by providing binding sites for ARF transcription factors, was activated in stem cells of plants expressing *MP* and *MPΔ* (6/8 independent T1 lines; Fig. 2h-j and Extended Fig. 5), suggesting that the resistance to auxin occurs, at least in part, downstream of ARF activity. Taken together, these experiments suggested that auxin signaling is locally gated to permit a low instructive output level, while at the same time protecting stem cells from the differentiation inducing effects of the phytohormone at high signaling levels.

WUSCHEL controls auxin signaling output in stem cells

Since suppressing auxin signaling output in stem cell caused SAM arrest and a phenotype highly similar to *wus* mutants (Fig. 2 k, l), we tested the contribution of *WUS* to controlling auxin responses in diverse genetic backgrounds. Since the *WUS* expression domain is massively enlarged in *clv* mutants[1,2], which causes stem cell over-proliferation phenotypes, SAMs from these plants provide an ideal background to elucidate the functional connection of WUS and auxin. Therefore, we analyzed auxin output in *clv3* meristems and found the DR5v2 minimum expanded in line with the overaccumulation of WUS, however some weak signal remained throughout the SAM (Fig. 3a, b). To test whether auxin signaling is required for stem cell over-proliferation in *clv3* mutants, we locally blocked auxin output by our *pCLV3:BDL-D* transgene and observed stem cell termination phenotypes in almost all seedlings (n=30; Fig. 3c). This result suggested that also in fasciated SAMs of *clv3* mutants, ectopic *WUS* is sufficient to reduce auxin signaling, while at the same time permitting basal output levels. To test the short term effect of enhancing WUS levels without the indirect effects of the *clv3* phenotype, we created plants that carry a *pUBI10:mCherry-GR-linker-WUS (WUS-GR)* transgene which allowed for experimental induction of ubiquitous WUS activity (Extended Fig. 6). After 24 h of DEX treatment the central auxin signaling minimum as well as the *CLV3* domain expanded (Extended Fig. 7), suggesting that WUS is indeed sufficient to reduce signaling output in the center of the SAM, but is unable to override active auxin responses at the periphery. To test whether *WUS* is also required to protect stem cells from high signaling levels, which lead to differentiation, we developed a genetic system that allowed us to inducibly remove WUS protein from stem cells. To this end, we adapted deGradFP technology[18] and combined switchable stem cell specific expression of an anti-GFP nanobody with a *pWUS:WUS-linker-GFP wus* rescue line[4]. After 24h of induction of nanobody expression, WUS-linker-GFP signal was substantially reduced in stem cells of the epidermis and subepidermis (Extended Fig. 8), while at the same time DR5v2 expression had spread into the center of the SAM (8/9 vs. 0/12 in control plants; Fig. 3 d, e). We made similar observations in plants carrying the weak *wus-7* allele, which are able to maintain a functional SAM for some time and only terminate stochastically. In these lines, DR5v2 activity fluctuated substantially and was frequently observed in the central zone (Extended Fig. 9). Taken together, these results demonstrated that WUS is required for stably maintaining stem cells in a state of low auxin signaling.

Mechanisms of auxin pathway gating

To address how WUS is able to gate the output of the auxin pathway, we went on to define direct target genes combining new ChIP-seq and RNA-seq experiments using seedlings of our *WUS-GR* line. Interestingly, WUS binding was almost exclusively found in regions of open chromatin[19] and among the WUS targets (Supplementary File 1 and refs. 20,21) we found the gene ontology term “response to auxin” to be most highly enriched within the developmental category (Extended Table 2). Importantly, WUS appeared to control auxin signaling output at all relevant levels, since it was able to bind to the promoters or regulate the expression of a large number of genes involved in auxin biosynthesis, transport, auxin perception, auxin signal transduction, as well as auxin response, which occurs downstream of ARF transcription factors (Fig. 4a and Extended Tables 3 and 4). Since WUS can act as transcriptional activator or repressor dependent on the regulatory environment[22,23] and our profiling results were based on ectopic expression of WUS in non-stem cells, we were unable to predict how the expression of individual targets would be affected *in vivo*. However, it has been reported that in the SAM, WUS mainly acts as a transcriptional repressor[20,22,24] and consistently, many auxin signaling components are expressed at high levels only in the periphery of the SAM and exhibit low RNA accumulation in the cells that are positive for WUS protein[12]. To test if WUS is required for this pattern, we analyzed the response of *MP* and *TIR1* mRNA accumulation to variations in *WUS* expression. To circumvent morphological defects of stable *wus* mutants, we again made use of our deGradFP line to analyze expression of *MP* after loss of WUS protein activity, but prior to changes in SAM morphology. After 24 h of induction, *MP* mRNA expression had extended from the periphery into the central zone (Fig. 4b, c; Extended Fig. 10, 11), demonstrating that WUS is indeed required for *MP* repression in stem cells. Conversely, ectopic activation of WUS revealed that it is also sufficient to reduce, but not shut down *MP* and *TIR1* transcription even in the periphery of the SAM (Fig. 4 d-e, Extended Fig. 7).

To elucidate the molecular mechanisms responsible for the observed regulatory gating, we asked whether chromatin structure may be changed in in response to WUS. WUS physically interacts with TOPLESS (TPL)[25,26], a member of the GROUCHO/Tup1 family of transcriptional co-repressors. These adaptor proteins mediate interaction with HISTONE DEACETYLASES (HDACs, reviewed in ref. 27), which in turn act to reduce transcriptional activity of chromatin regions via promoting the removal of acetyl modifications from histone tails[28]. To test whether regulation of chromatin modification

is involved in translating WUS activity into the observed reduction of transcriptional activity of target genes we quantified histone acetylation on H3K9 and methylation on H3K27. After 2 h of induction of our *WUS-GR* line, we observed a significant change in the genome wide histone acetylation patterns, which were spatially correlated with WUS chromatin binding events (2939 out of 6740 WUS bound chromatin regions showed acetylation changes), while histone methylation patterns were largely unaffected (525 out of 6740 WUS bound chromatin regions showed methylation changes). WUS binding events clustered in the proximal promoter regions, while chromatin regions whose acetylation levels were changed after WUS activation were mainly found around the transcriptional start sites and 5´UTRs of genes (Fig. 4f). Zooming in on the 1656 directly repressed WUS targets, we found that 587 of them also showed histone de-acetylation. For the vast majority of these loci the observed reduction was fairly subtle, suggesting that mild de-acetylation may be the mechanism that allows WUS to reduce, but not shut off transcription of target genes. To test whether the observed changes in chromatin state of direct WUS targets also translate to variation in gene expression, we induced WUS activity in the presence of Trichostatin A (TSA), a potent inhibitor of class I and II HDACs[29], and recorded the transcriptional response. Strikingly, from the 1656 directly repressed genes, 922 were no longer responsive to WUS-GR induction when TSA was present, underlining the relevance of histone de-acetylation for the genome-wide functional output of WUS. To investigate whether this mechanism is relevant for controlling auxin responses in the SAM, we analyzed DR5v2 reporter activity after TSA and/or auxin treatment. Auxin was insufficient to trigger a transcriptional response in stem cells, likely due to the presence of functional WUS (Fig. 4g). In contrast, inactivation of HDACs and consequently WUS-mediated transcriptional repression by TSA treatment, led to low but consistent DR5v2 signal in the center of the meristem (Fig. 4h). Combining stimulation of the pathway with reduction in WUS function caused substantial DR5v2 response in stem cells (Fig. 4i). Taken together, these results showed that WUS binds to and reduces transcription of the majority of genes involved in auxin signaling and response via de-acetylation of histones and thus is able to maintain pathway activity in stem cells at a basal level.

Pathway wide gating provides robustness to apical stem cell fate

We next wondered what the functional relevance of the observed pathway wide regulatory interaction might be. Therefore, we tested the capacity of WUS targets with auxin signaling or response functions to interfere with stem cell activity. Based on their highly localized expression at the periphery of the SAM[12], we selected the signaling components *ARF3*, *ARF4*, *ARF5* (*MP)*, *IAA8*, *IAA9*, and *IAA12* (*BDL)* as well as the TIR1 receptor along with transcription factors of the auxin response category including *TARGET OF MONOPTEROS* (*TMO*) and *LATERAL ORGAN BOUNDARIES* (*LOB*) genes that have established roles in other developmental contexts[30]. Neither of the 17 factors tested caused meristem phenotypes when expressed in stem cells (Fig. 2 and Extended Table 5), highlighting the robustness of stem cell fate in the presence of WUS on the one hand and the activity of auxin signaling in these cells on the other hand. This conclusion is based on two observations: 1. The auxin sensitive native version of BDL was unable to terminate the SAM in contrast to the auxin insensitive BDL-D version (Fig. 2i, j). 2. *pCLV3:MP* plants showed enhanced DR5v2 activity in stem cells (Fig. 2g, h) demonstrating that ARF activity is indeed limiting for transcriptional output in wild-type. However, this transcriptional output registered by the DR5v2 reporter is not translated into an auxin response, since WUS limits the expression of a large fraction of the required downstream genes (Fig. 4a; extended tables 2, 3). Thus, WUS seems to act both up- and downstream of the key ARF transcription factors.

Since we had found that stem cell specific expression of individual auxin signaling components was not sufficient to interfere with stem cell fate, we wanted to test whether reducing *WUS* function would sensitize stem cells to activation of the entire pathway. To this end, we grew plants segregating for *wus-7* on plates supplemented with auxin. Eleven days after germination, we observed twice as many terminated *wus-7* mutant seedlings than on control plates, whereas wild-type seedlings were unaffected (Fig. 3f, Extended Fig. 12). Thus, reducing *WUS* function allowed activation of auxin responses under conditions that were tolerated in wild type. Taken together, the activation of individual pathway components was insufficient to override the protective effect of WUS, however removing the master regulator itself rendered stem cells vulnerable to even mild perturbations in auxin signaling.

Discussion

In conclusion, our results show that WUS restricts auxin signaling in apical stem cells by pathway-wide transcriptional control, while at the same time allowing instructive low levels of signaling output. This rheostatic activity may be based on selective transcriptional repression/activation of a subset of signaling and response components that render the pathway unresponsive to high input levels. Alternatively, WUS may be able to reduce expression of targets rather than to shut off their activity completely, leaving sufficient capacity for low level signaling only. In support of the latter hypothesis, we demonstrate that WUS acts via de-acetylation of histones and that interfering with HDAC activity triggers auxin responses in stem cells. However, there is evidence supporting both scenarios[20-23] and likely both mechanisms work hand in hand dependent on the regulatory environment of the individual cell. Thus, a definitive answer will require inducible WUS loss of function approaches in stem cells coupled with time-resolved whole genome transcript profiling at the single cell level. Importantly, in addition to its effects on auxin signaling, WUS enhances cytokinin responses via the repression of negative feedback regulators[24]. Whereas this interaction can be overridden by expression of dominant cytokinin signaling components[24], stem cells remain unresponsive to elements of the auxin pathway. This argues that the regulation of the auxin pathway might be of higher significance than the interaction with cytokinin, which may primarily serve to sustain *WUS* expression[31,32]. Auxin and cytokinin signaling are directly coupled[17] and balancing their outputs is key to maintaining functional plant stem cell niches[17,33]. Given the dynamic and self-organizing nature of the auxin system[34], the independent spatial input provided by WUS appears to be required to bar differentiation competence from the center of the SAM, while at the same time still allowing to sense this important signal. In light of the recent findings that PIN1 mediated auxin flux in the SAM is directed towards the center[35], it is tempting to speculate that auxin may serve as a positional signal not only for organ initiation, but also for stem cells.

Author Contributions:

A. Me. performed in situ hybridizations, C.W. carried out imaging and analyses, J.F. established the WUS-GR line, G.U. and A. M. performed RNA-seq, O.E. performed bioinformatic analyses, K.B. and T.G. established the *pDR5v2:ER-EYFP-HDEL:tAt4g24550* line, C.G. made the *pCLV3:mCherry-NLS:tCLV3* construct, Z.Š., A.M and Y.M. performed all other experiments. C.G.-A. and T.V. designed the TSA treatment of the SAM, Y.M., Z.Š., A.M. and J.U.L. designed all other experiments and wrote the paper with input from all other authors.

Acknowledgments:

We thank Dolf Weijers for sharing R2D2 and DR5v2 resources before publication. This work was supported by the DFG through grants SFB1101 and SFB873 to JUL and TG and by HFSP Grant RPG0054-2013 and ANR-12-BSV6-0005 grant to T.V. Computational analyses have been carried out on heiCLOUD provided by Heidelberg University Computing Centre.

References

1. Schoof, H. *et al.* The stem cell population of Arabidopsis shoot meristems in maintained by a regulatory loop between the CLAVATA and WUSCHEL genes. *Cell* **100,** 635–644 (2000).
2. Brand, U., Fletcher, J. C., Hobe, M., Meyerowitz, E. M. & Simon, R. Dependence of stem cell fate in Arabidopsis on a feedback loop regulated by CLV3 activity. *Science* **289,** 617–619 (2000).
3. Yadav, R. K. *et al.* WUSCHEL protein movement mediates stem cell homeostasis in the Arabidopsis shoot apex. *Genes Dev* **25,** 2025–2030 (2011).
4. Daum, G., Medzihradszky, A., Suzaki, T. & Lohmann, J. U. A mechanistic framework for noncell autonomous stem cell induction in Arabidopsis. *Proc Natl Acad Sci USA* **111,** 14619–14624 (2014).
5. Benjamins, R. & Scheres, B. Auxin: the looping star in plant development. *Annu Rev Plant Biol* **59,** 443–465 (2008).
6. Kepinski, S. & Leyser, O. Auxin-induced SCFTIR1-Aux/IAA interaction involves stable modification of the SCFTIR1 complex. *Proc. Natl. Acad. Sci. U.S.A.* **101,** 12381–12386 (2004).
7. Dharmasiri, N., Dharmasiri, S. & Estelle, M. The F-box protein TIR1 is an auxin receptor. *Nature* **435,** 441–445 (2005).
8. Kepinski, S. & Leyser, O. The Arabidopsis F-box protein TIR1 is an auxin receptor. *Nature* **435,** 446–451 (2005).
9. Vernoux, T., Kronenberger, J., Grandjean, O., Laufs, P. & Traas, J. PIN-FORMED 1 regulates cell fate at the periphery of the shoot apical meristem. *Development* **127,** 5157–5165 (2000).
10. Reinhardt, D. *et al.* Regulation of phyllotaxis by polar auxin transport. *Nature* **426,** 255–260 (2003).
11. Liao, C.-Y. *et al.* Reporters for sensitive and quantitative measurement of auxin response. *Nature Methods* **12,** 207–210 (2015).
12. Vernoux, T. *et al.* The auxin signalling network translates dynamic input into robust patterning at the shoot apex. *Mol Syst Biol* **7,** 508 (2011).
13. Brunoud, G. *et al.* A novel sensor to map auxin response and distribution at high spatio-temporal resolution. *Nature* **482,** 103–106 (2012).
14. Vatén, A. *et al.* Callose biosynthesis regulates symplastic trafficking during root development. *Dev Cell* **21,** 1144–1155 (2011).
15. Lloyd, A. M., Schena, M., Walbot, V. & Davis, R. W. Epidermal cell fate determination in Arabidopsis: patterns defined by a steroid-inducible regulator. *Science* **266,** 436–439 (1994).
16. Hardtke, C. S. & Berleth, T. The Arabidopsis gene MONOPTEROS encodes a transcription factor mediating embryo axis formation and vascular development. *EMBO J* **17,** 1405–1411 (1998).
17. Zhao, Z. *et al.* Hormonal control of the shoot stem-cell niche. *Nature* **465,** 1089–1092 (2010).
18. Caussinus, E., Kanca, O. & Affolter, M. Fluorescent fusion protein knockout mediated by anti-GFP nanobody. *Nature Publishing Group* **19,** 117–121 (2011).
19. Zhang, W., Zhang, T., Wu, Y. & Jiang, J. Genome-wide identification of regulatory DNA elements and protein-binding footprints using signatures of open chromatin in Arabidopsis. *Plant Cell* **24,** 2719–2731 (2012).
20. Busch, W. *et al.* Transcriptional control of a plant stem cell niche. *Dev Cell* **18,** 849–861 (2010).

21. Yadav, R. K. *et al.* Plant stem cell maintenance involves direct transcriptional repression of differentiation program. *Mol Syst Biol* **9,** 654–654 (2013).
22. Ikeda, M., Mitsuda, N. & Ohme-Takagi, M. Arabidopsis WUSCHEL is a bifunctional transcription factor that acts as a repressor in stem cell regulation and as an activator in floral patterning. *Plant Cell* **21,** 3493–3505 (2009).
23. Zhou, Y. *et al.* HAIRY MERISTEM with WUSCHEL confines CLAVATA3 expression to the outer apical meristem layers. *Science* **361,** 502–506 (2018).
24. Leibfried, A. *et al.* WUSCHEL controls meristem function by direct regulation of cytokinin-inducible response regulators. *Nature* **438,** 1172–1175 (2005).
25. Long, J. A., Ohno, C., Smith, Z. R. & Meyerowitz, E. M. TOPLESS regulates apical embryonic fate in Arabidopsis. *Science* **312,** 1520–1523 (2006).
26. Kieffer, M. *et al.* Analysis of the transcription factor WUSCHEL and its functional homologue in Antirrhinum reveals a potential mechanism for their roles in meristem maintenance. *Plant Cell* **18,** 560–573 (2006).
27. Liu, Z. & Karmarkar, V. Groucho/Tup1 family co-repressors in plant development. *Trends Plant Sci* **13,** 137–144 (2008).
28. Taunton, J., Hassig, C. A. & Schreiber, S. L. A mammalian histone deacetylase related to the yeast transcriptional regulator Rpd3p. *Science* **272,** 408–411 (1996).
29. Yoshida, M., Kijima, M., Akita, M. & Beppu, T. Potent and specific inhibition of mammalian histone deacetylase both in vivo and in vitro by trichostatin A. *J Biol Chem* **265,** 17174–17179 (1990).
30. Schlereth, A. *et al.* MONOPTEROS controls embryonic root initiation by regulating a mobile transcription factor. *Nature* **464,** 913–916 (2010).
31. Gordon, S. P., Chickarmane, V. S., Ohno, C. & Meyerowitz, E. M. Multiple feedback loops through cytokinin signaling control stem cell number within the Arabidopsis shoot meristem. *Proceedings of the National Academy of Sciences* **106,** 16529–16534 (2009).
32. Buechel, S. *et al.* Role of A-type ARABIDOPSIS RESPONSE REGULATORS in meristem maintenance and regeneration. *European Journal of Cell Biology* **89,** 279–284 (2010).
33. Müller, B. & Sheen, J. Cytokinin and auxin interaction in root stem-cell specification during early embryogenesis. *Nature* **453,** 1094–1097 (2008).
34. Bhatia, N. *et al.* Auxin Acts through MONOPTEROS to Regulate Plant Cell Polarity and Pattern Phyllotaxis. *Curr Biol* **26,** 3202–3208 (2016).
35. Galván-Ampudia, C. S. *et al.* From spatio-temporal morphogenetic gradients to rhythmic patterning at the shoot apex. BioRxiv (2018).
36. Yadav, R. K., Tavakkoli, M., Xie, M., Girke, T. & Reddy, G. V. A high-resolution gene expression map of the Arabidopsis shoot meristem stem cell niche. *Development* **141,** 2735–2744 (2014).
37. Yadav, R. K., Girke, T., Pasala, S., Xie, M. & Reddy, G. V. Gene expression map of the Arabidopsis shoot apical meristem stem cell niche. *Proc Natl Acad Sci USA* **106,** 4941–4946 (2009).
38. Prunet, N. Live Confocal Imaging of Developing Arabidopsis Flowers. *J Vis Exp* e55156–e55156 (2017). doi:10.3791/55156
39. Roslan, H. A. *et al.* Characterization of the ethanol-inducible alc gene-expression system in Arabidopsis thaliana. **28,** 225–235 (2001).
40. Lampropoulos, A. *et al.* GreenGate---a novel, versatile, and efficient cloning system for plant transgenesis. *PLoS ONE* **8,** e83043 (2013).
41. Schindelin, J. *et al.* Fiji: an open-source platform for biological-image analysis. *Nat Meth* **9,** 676–682 (2012).

42. de Reuille, P. B., Robinson, S. & Smith, R. S. Quantifying cell shape and gene expression in the shoot apical meristem using MorphoGraphX. *Methods Mol Biol* **1080,** 121–134 (2014).
43. Sommer, C., Straehle, C., Kothe, U. & Hamprecht, F. A. Ilastik: Interactive learning and segmentation toolkit. in 230–233 (IEEE, 2011). doi:10.1109/ISBI.2011.5872394
44. Berthold, M. R. *et al.* KNIME - the Konstanz information miner: version 2.0 and beyond. *ACM SIGKDD Explorations Newsletter* **11,** 26–31 (2009).
45. Medzihradszky, A., Schneitz, K. & Lohmann, J. U. Detection of mRNA expression patterns by nonradioactive in situ hybridization on histological sections of floral tissue. *Methods Mol Biol* **1110,** 275–293 (2014).
46. Pfeiffer, A. *et al.* Integration of light and metabolic signals for stem cell activation at the shoot apical meristem. *Elife* **5,** 827 (2016).
47. Li, H. & Durbin, R. Fast and accurate short read alignment with Burrows-Wheeler transform. *Bioinformatics* **25,** 1754–1760 (2009).
48. Afgan, E. *et al.* The Galaxy platform for accessible, reproducible and collaborative biomedical analyses: 2018 update. *Nucleic Acids Res* **46,** W537–W544 (2018).
49. Starmer, J. & Magnuson, T. Detecting broad domains and narrow peaks in ChIP-seq data with hiddenDomains. *BMC Bioinformatics* **17,** 144 (2016).
50. Huang, W., Loganantharaj, R., Schroeder, B., Fargo, D. & Li, L. PAVIS: a tool for Peak Annotation and Visualization. *Bioinformatics* **29,** 3097–3099 (2013).
51. Kim, D., Langmead, B. & Salzberg, S. L. HISAT: a fast spliced aligner with low memory requirements. *Nat Meth* **12,** 357–360 (2015).
52. Liao, Y., Smyth, G. K. & Shi, W. featureCounts: an efficient general purpose program for assigning sequence reads to genomic features. *Bioinformatics* **30,** 923–930 (2014).
53. Love, M. I., Huber, W. & Anders, S. Moderated estimation of fold change and dispersion for RNA-seq data with DESeq2. *Genome Biol* **15,** 550 (2014).

Figures and Legends:

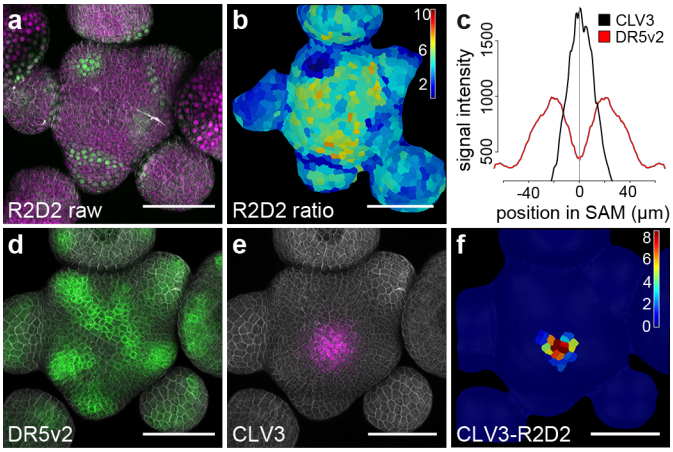

Figure 1: Auxin output minimum correlates with apical stem cells.

a) Confocal readout from R2D2 auxin input sensor. **b**) Ratiometric representation of R2D2 activity in the epidermal cell layer (L1). **c**) Quantification of averaged *pDR5v2:ER-eYFP-HDEL* and *pCLV3:mCherry-NLS* distribution (n=5). **d**) Confocal readout from *pDR5v2:ER-eYFP-HDEL* auxin output reporter. **e**) *pCLV3:mCherry-NLS* stem cell marker in the same SAM. **f**) Computational subtraction of L1 signals shown in (d) and (e). Relative signal intensity is shown in arbitrary units. All scale bars, 50 *µ*m.

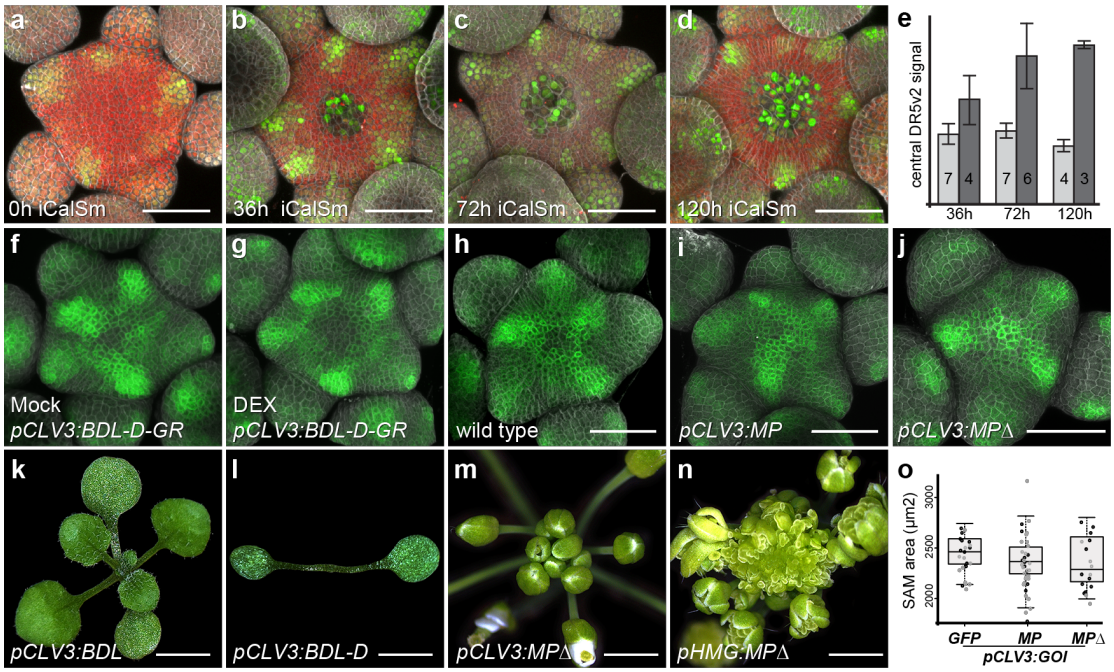

Fig. 2: Apical stem cells are dependent on auxin signaling, but resistant to differentiation.

a-d) *pDR5v2:3xVENUS-NLS* activity after induction of iCalSm. Stem cell differentiation is marked by loss of *pRPS5a:NLS-tdTomato.* **e)** Quantification of DR5v2 signal intensity in the central zone across the experimental cohort. Light grey bars represent uninduced controls, dark grey bars represent plants induced with 1% ethanol. Numbers of analyzed SAMs are indicated. See also Extended Figure 1-3 and Extended Table 1. **f-j**) *pDR5v2:ER-eYFP-HDEL* activity in plants harboring *pCLV3:BDL-D-GR* after 24h of mock treatment (f), *pCLV3:BDL-D-GR* after 24h of DEX treatment (g), wild type (h), *pCLV3:MP* (i) or *pCLV3:MPΔ* (j). **k-n**) Representative phenotypes of lines expressing *pCLV3:BDL* (k), *pCLV3:BDL-D* (l), *pCLV3:MPΔ* (m), or *pHMG:MPΔ* (n). **o)** SAM size quantifications for plants carrying *pCLV3:GFP, pCLV3:MP,* or *pCLV3:MPΔ* in two independent T1 populations. All scale bars 50 µm, except k) and i) 3,5 mm; m) and n) 2mm.

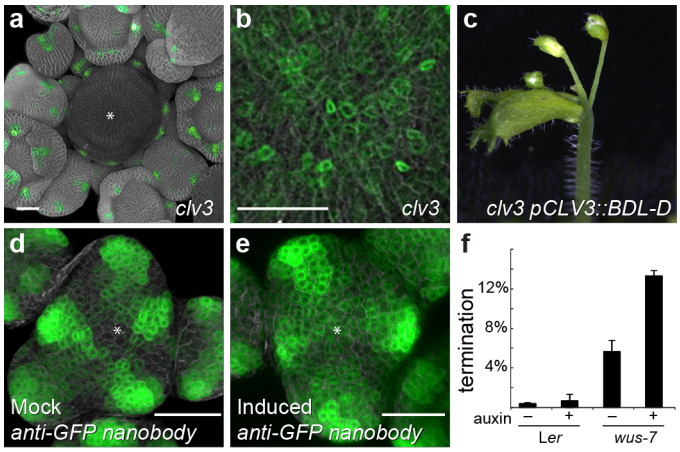

Fig. 3: WUSCHEL maintains low auxin signaling output in stem cells.

a) *pDR5v2:ER-mCherry-HDEL* activity in SAM of *clv3* mutant. Asterisk marks center of SAM. **b**) Zoom into central SAM area of *clv3* mutants reveals basal *pDR5v2* activity. **c**) SAM arrest caused by *pCLV3:BDL-D* expression in *clv3*. **d, e**) Representative *pDR5v2:ER-mCherry-HDEL* signals after 24h of mock treatment (d) or inducible depletion of WUS protein from stem cells by ethanol induction (e). **f**) Quantification of terminated seedlings grown on auxin plates (10 μM IAA; n > 200 for each genotype and treatment). Genotyping revealed that all arrested plants were homozygous for *wus-7*. Scale bars, 50 μm.

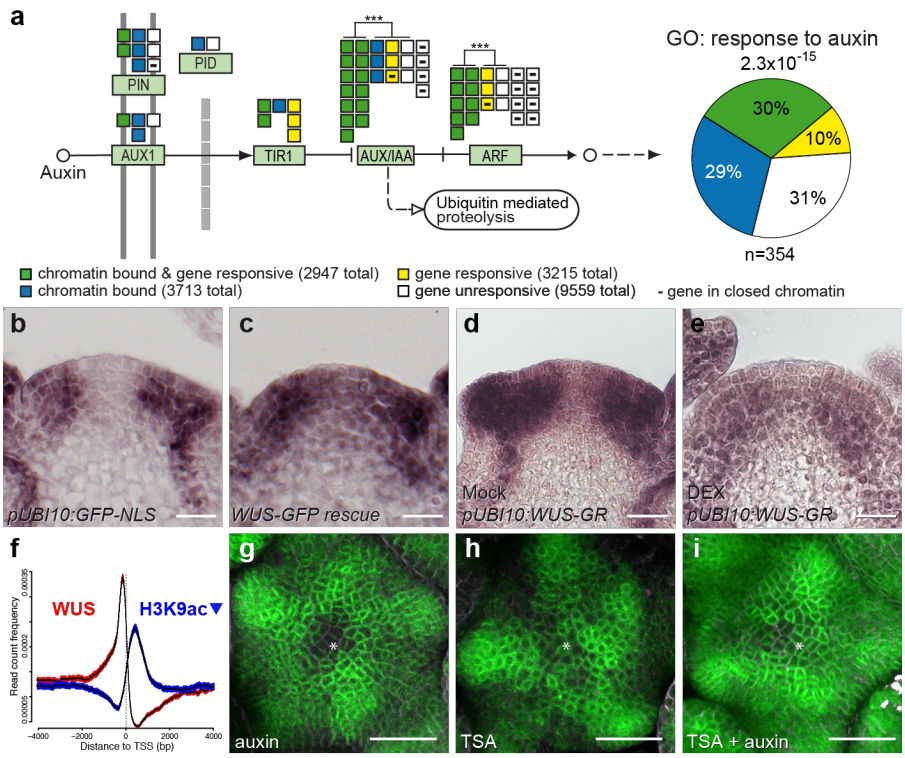

Fig. 4: Pathway level control underlies WUSCHEL mediated gating of auxin signaling.

a) WUS globally affects the auxin pathway, including transport, perception, signal transduction, as well as transcriptional response. Across the entire pathway bound and responsive genes are overrepresented (p-value $9.9*10^{-10}$). Within gene family tests are shown. *** p-value by Fisher exact test < 10^{-4}. **b, c**) *MP* RNA accumulation 24 hours post anti-GFP nanobody induction in **b**) a *pUBI10:GFP-NLS* control line and **c)** the *pWUS:WUS-linker-GFP wus* rescue background. **d, e**) Response of *MP* mRNA to induction of WUS-GR. *MP* RNA after 24h of mock (d) or DEX treatment (e). **f)** Spatial correlation between WUS chromatin binding events (red) and regions with reduced histone acetylation (blue) 0.95 confidence intervals are shown. **g-i**) Representative images of *pDR5v2:ER-mCherry-HDEL* activity in response to HDAC inhibition. **g)** auxin treated SAM; **h)** TSA treated SAM; **i)** TSA and auxin treated SAM. Scale bars b-e: 20μm; g-i: 30μm.

Extended Data

Extended Figures 1-12

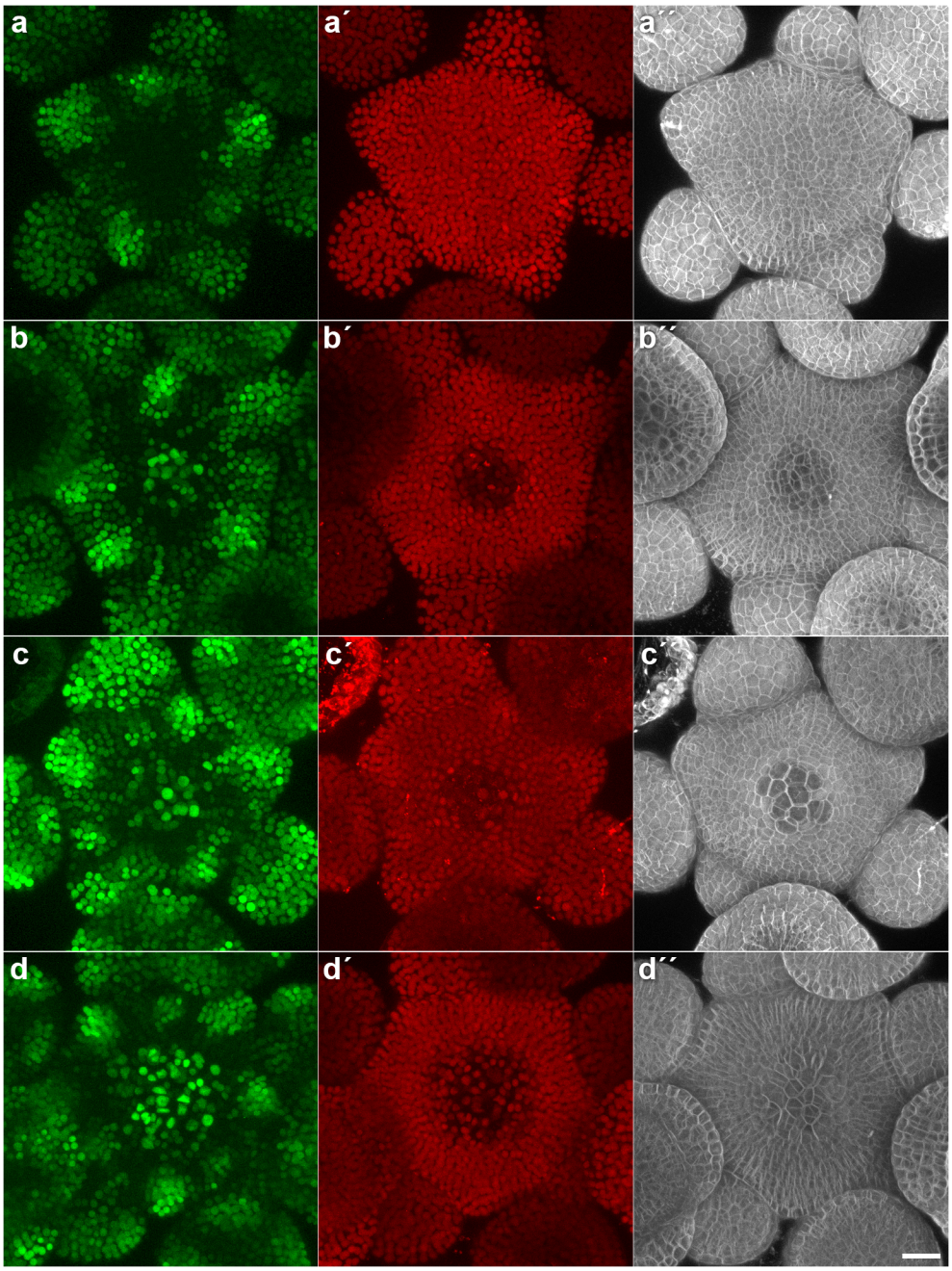

Extended Figure 1: Activation of DR5v2 and differentiation after induced stem cell loss.

Representative SAMs of the imaged cohorts quantified in Extended Table 1. **a)** 0h after induction **b)** 36h after induction **c)** 72h after induction **d)** 120h after induction. Left panels show *pDR5v2:3xVENUS-NLS* signal, middle panels show *pRPS5a:NLS-tdTomato* and right panels show DAPI stained cell walls. Scale bars, 20μm.

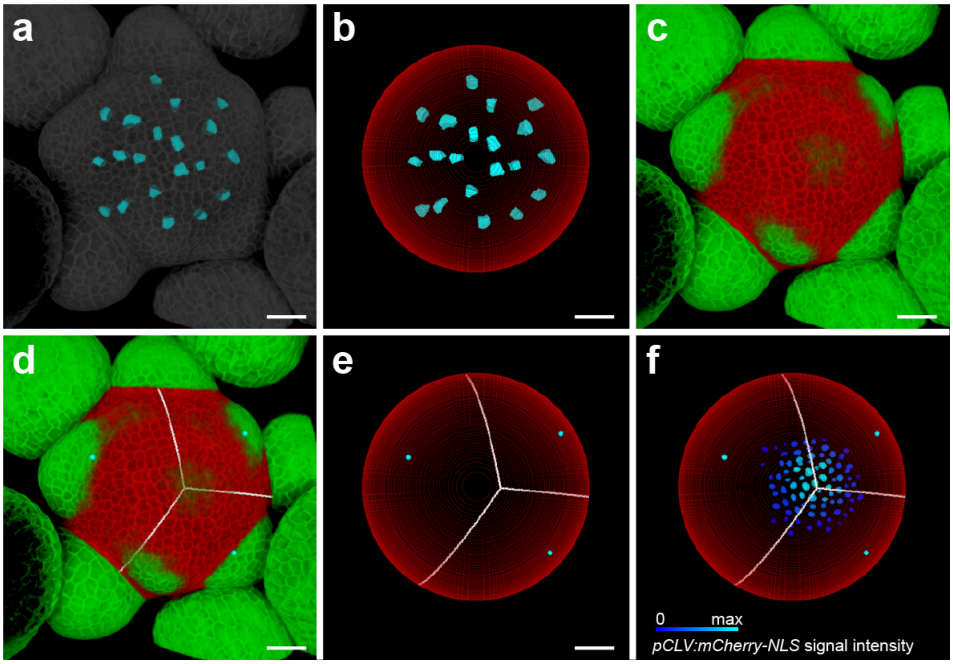

Extended Figure 2: Computational strategy to identify the stem cell domain.

a) In a first step, cells across the L1 of the SAM are segmented. **b)** Based on the position of segmented cells, a perfect sphere is fitted to the SAM. **c)** The sphere is applied to the SAM and organ primordia are identified by emergence through the sphere. **d, e)** Equidistant points between the primordia are calculated and used to triangulate the center of the SAM. **f)** The triangulated center was benchmarked against SAMs haboring *pCLV3* reporter labelled stem cells (n=9). The triangulation invariantly identified one of the most central *pCLV3* positive cells. See also Methods. Scale bars, 20μm.

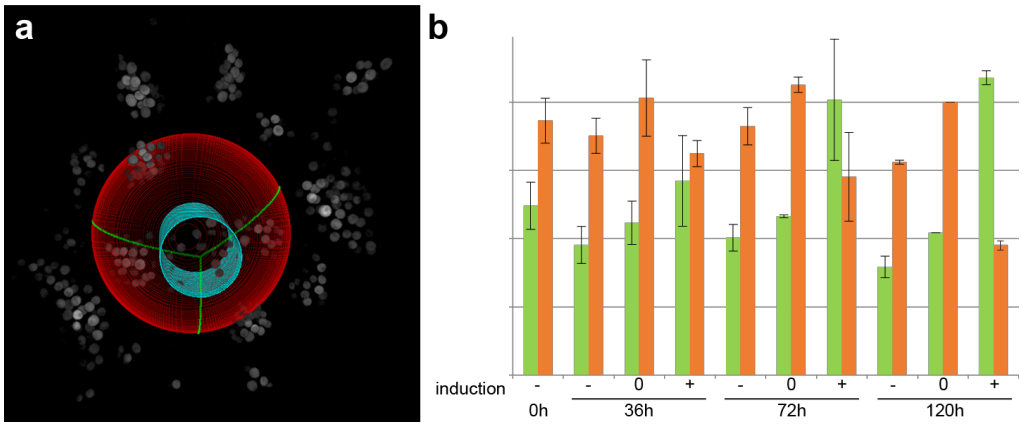

Extended Figure 3: Quantification of signal changes in the stem cell domain following induced stem cell loss.

a) For signal quantification in the stem cell domain, a cylinder with radius r_{cyl} (= 1/3 * r_{sphere}) mimicking the average size of the *CLV3* domain was placed into the computationally identified center of the SAM and fluorescence intensities were quantified within this narrowly defined subdomain. DR5v2-NLS signals are shown in grey, SAM sphere derived from segmentation in red, triangulation lines in green and quantification cylinder in cyan. **b)** Quantification of fluorescent signals from all SAMs of the stem cell loss experiment described in Extended Table 1. Total fluorescence signal intensities for *pDR5v2:3xVENUS-NLS* and *pRPS5a:NLS-tdTomato* for the inner region (I_{cyl}) and for the peripheral region (I_{sphere}) were extracted from respective image volumes. I_{cyl} was averaged over all plants for each time-point and condition and normalized to the overall signal (I_{cyl} + I_{sphere}).

Green bars: DR5v2:3xVENUS-NLS signal, Orange bars: pRPS5a:NLS-tdTomato signal. - : mock treated, 0: ethanol induced, but no observable stem cell loss, + : ethanol induced and stem cell loss.

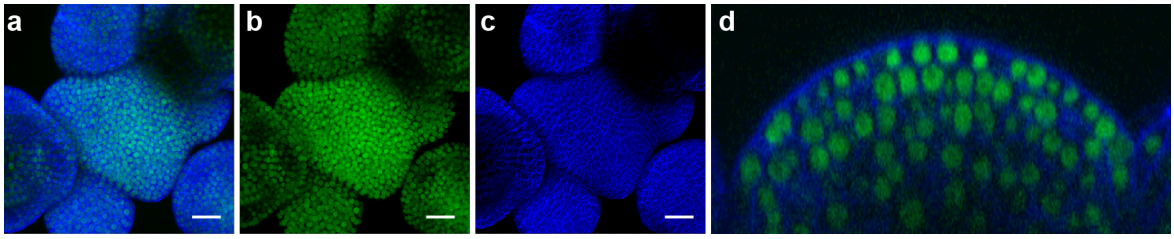

Extended Figure 4: Activity of the *pHMG* promoter.

Transgenic line carrying 1347 bp upstream of the At1g76110 locus fused to the *GFP-NLS* coding sequence. **a)** GFP and DAPI channels. **b)** GFP channel. **c)** DAPI channel. **d)** Side view though a representative SAM. Scale bars, 20 μm.

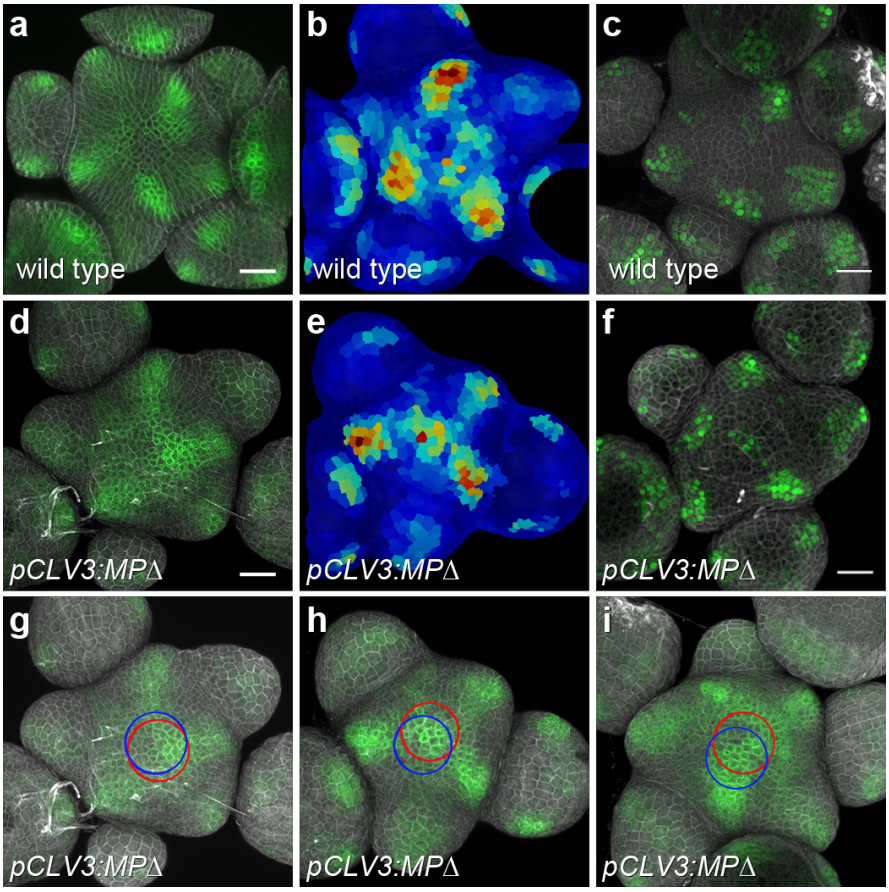

Extended Figure 5: Auxin signaling output in wild type and *pCLV3:MPΔ* lines.

a) *pDR5v2:ER-EYFP-HDEL* in wild type **b)** Quantification of an independent *pDR5v2:ER-EYFP-HDEL* wild-type SAM **c)** *pDR5v2:3xVENUS-NLS* in wild type **d-f)** Auxin signaling output was present in the centre of *pCLV3:MPΔ* lines, indicated by two independent reporters *pDR5v2:ER-EYFP-HDEL* (6 out of 8 independent T1 plants) (d) and *pDR5v2:3xVENUS-NLS* (6 out of 7 independent T1 plants) (f). **e)** Quantification of *pDR5v2:ER-EYFP-HDEL* in an independent *pCLV3:MPΔ* SAM. DR5v2 activity was not observed in the center of wild-type SAMs grown in the same experiments. **g-i)** Computationally derived central zone in L1 (red) and L3 (blue) are superimposed to SAMs of *pDR5v2:ER-EYFP-HDEL* carrying *pCLV3:MPΔ* (g, h) and *pCLV3:MP* (i). DR5v2 signal clearly coincides with central zone. Scale bars, 20μm.

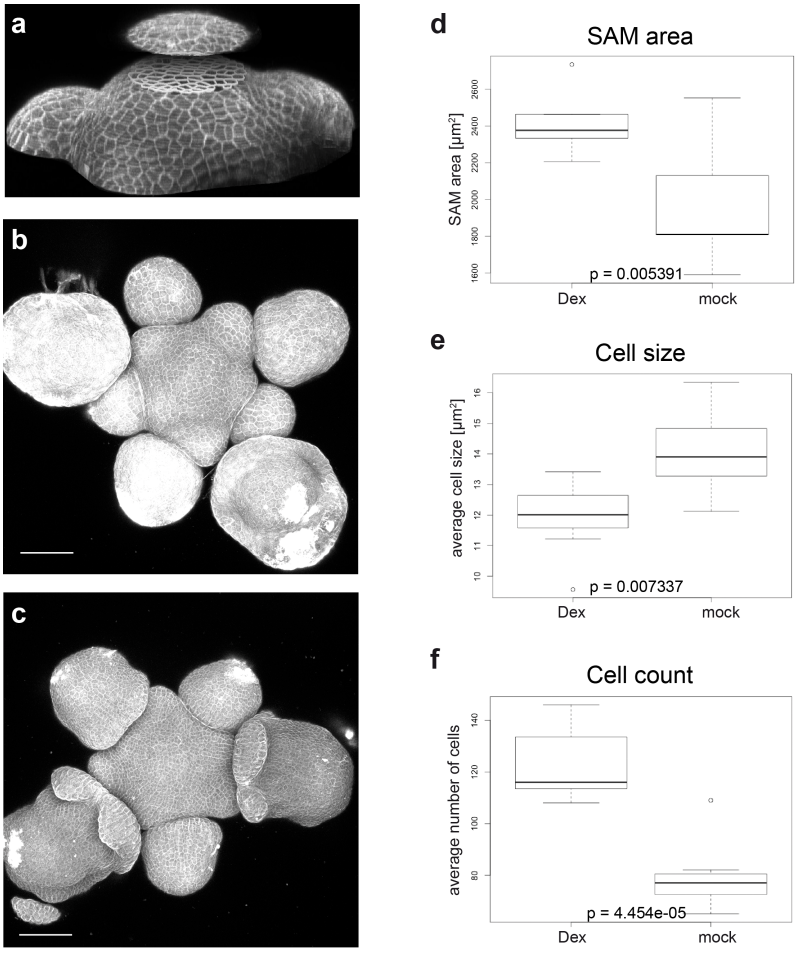

Extended Figure 6: Morphological effects of WUS-GR induction.

a) Visualization of meristem morphology analysis strategy. Meristem size, cell count and average cell size were measured at a constant relative position defined by the image plane in which the L1 to L2 transition became visible. **b)** Mock treated and **c)** DEX induced *pUBI:mCherry-GR-linker-WUS* SAMs four days after local application. Following WUS induction, SAM size increased **(d)**, cell size decreased **(e)** and cell number strongly increased **(f)** n= 7 and 8 meristems, respectively. Scale bars, 50 μm.

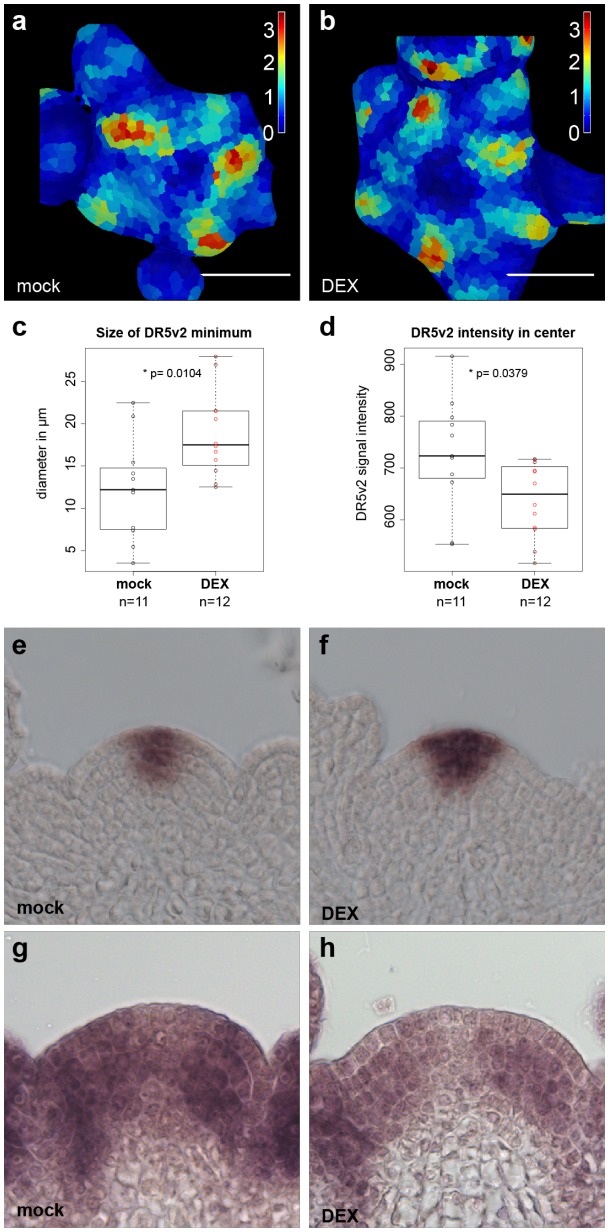

Extended Figure 7: SAM specific molecular responses to ectopic WUS induction.

24 hours after induction of ectopic WUS-GR activity, DR5v2 signal in the central zone was supressed and *CLV3* mRNA expression was enhanced. Representative in situ quantifications of DR5v2 signal after mock **(a)** and DEX **(b)** treatments. **c)** Quantification of the size of the central DR5v2 minimum. **d)** Quantification of the average DR5v2 signal intensity in the central zone. **e)** *CLV3* mRNA expression after 24 hours of mock treatment. **f)** *CLV3* mRNA expression after 24 hours of DEX treatment. **g)** *TIR1* mRNA expression after 24 hours of mock treatment. **h)** *TIR1* mRNA expression after 24 hours of DEX treatment. SAMs of both treatment types were hybridized on the same microscopic slide and imaged under identical settings.

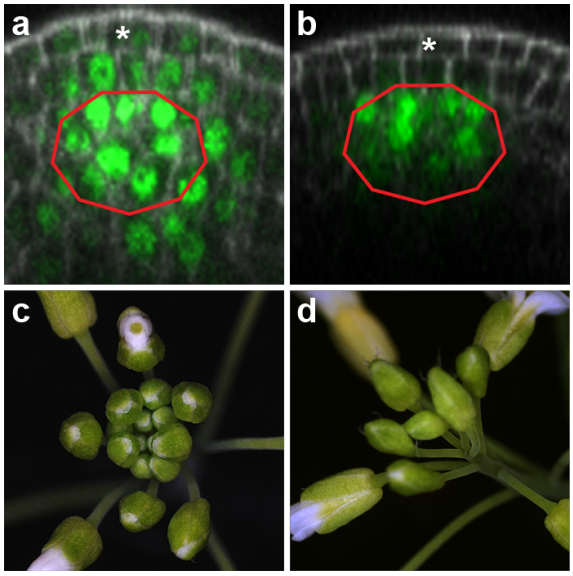

Extended Figure 8: Inducible depletion of WUS protein by stem cell expressing anti-GFP nanobody.

Representative images of a *pWUS:WUS-linker-GFP* rescue line expressing the anti GFP nanobody under the control of *pCLV3:AlcR*. The full genotype of these plants was: *wus/pWUS:WUS-linker-GFP/pCLV3:AlcR/pAlcA:NSImb-vhhGFP4*. **a)** WUS-linker-GFP signal after 24h of mock treatment. **b)** WUS-linker-GFP signal after 24h of induction with 1% ethanol. Shoot phenotypes after five days of mock **(c)** or ethanol induction **(d)**. Red line marks *WUS* mRNA expressing cells of the organizing centre; asterisk denotes epidermal stem cell.

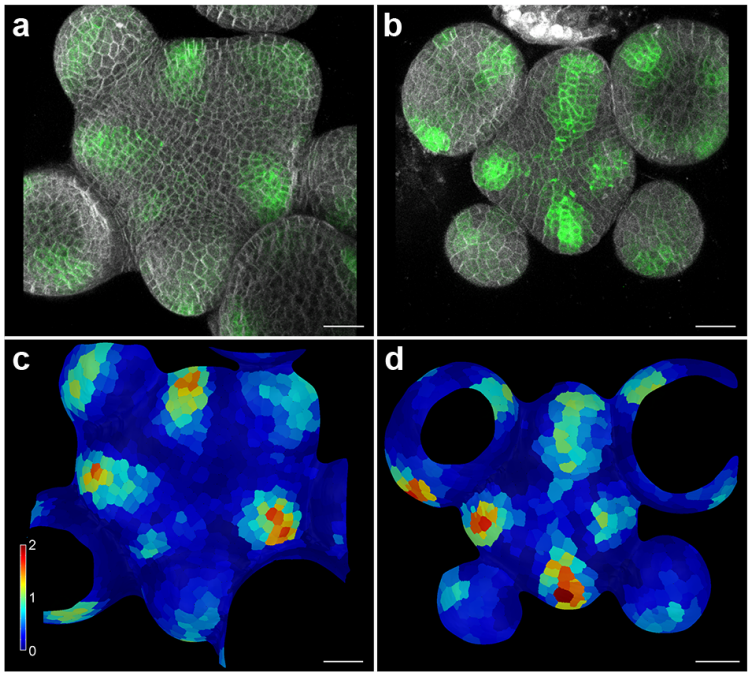

Extended Figure 9: SAMs of *wus-7* plants show auxin signaling output in the stem cell domain.

a) Representative image of *pDR5v2:ER-eYFP-HDEL* signal in the SAM of L*er* wild-type plants. Only 16% of plants showed DR5v2 activity in the center of the SAM (n=38). **b)** Representative image of *pDR5v2:ER-eYFP-HDEL* signal in a *wus-7* SAM before termination. 61% of *wus-7* plants showed DR5v2 activity in the center of the SAM (n=13). Per cell quantification of DR5v2 signal in wild type (**c**) and *wus-7* (**d**). Scale bars, 20 μm

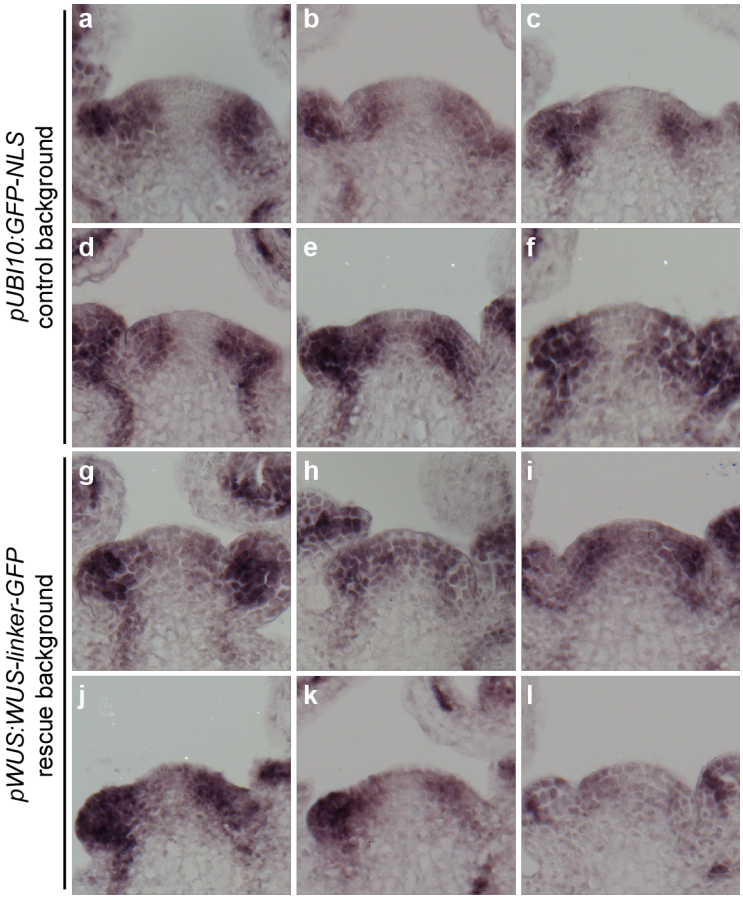

Extended Figure 10: *MP* mRNA expression after induced WUS loss of function. Experiment I.

a-f) In situ detection of *MP* mRNA in *pUBI10:GFP-NLS* control plants carrying *pCLV3:AlcR/AlcA:NSlmb-vhhGFP4* after 24h of ethanol treatment. **g-l)** In situ detection of *MP* mRNA in stable *pWUS:WUS-linker-GFP wus* rescue plants carrying *pCLV3:AlcR/AlcA:NSlmb-vhhGFP4* after 24h of ethanol treatment. SAMs of both genotypes were hybridized in a single experiment and imaged under identical settings. Unadjusted images are shown.

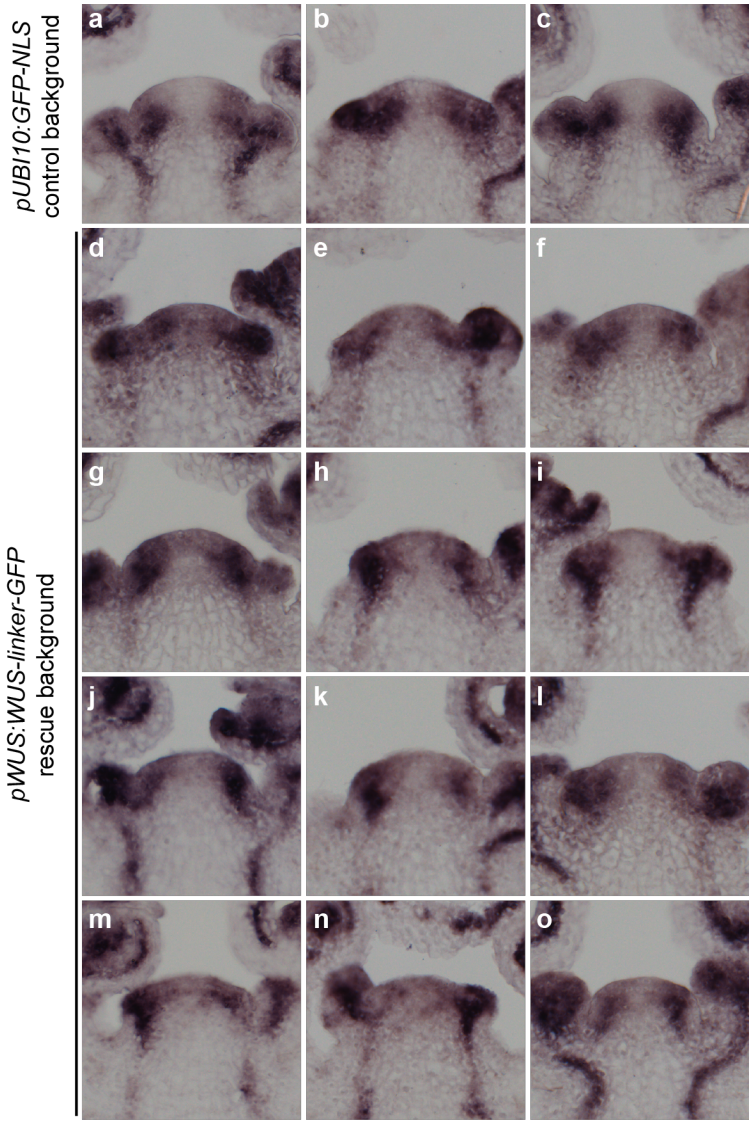

Extended Figure 11: *MP* mRNA expression after induced WUS loss of function. Experiment II.

a-c) In situ detection of *MP* mRNA in *pUBI10:GFP-NLS* control plants carrying *pCLV3:AlcR/AlcA:NSlmb-vhhGFP4* after 24h of ethanol treatment. **d-o)** In situ detection of *MP* mRNA in stable *pWUS:WUS-linker-GFP wus* rescue plants carrying *pCLV3:AlcR/AlcA:NSlmb-vhhGFP4* after 24h of ethanol treatment. SAMs of both genotypes were hybridized in a single experiment and imaged under identical settings. Unadjusted images are shown.

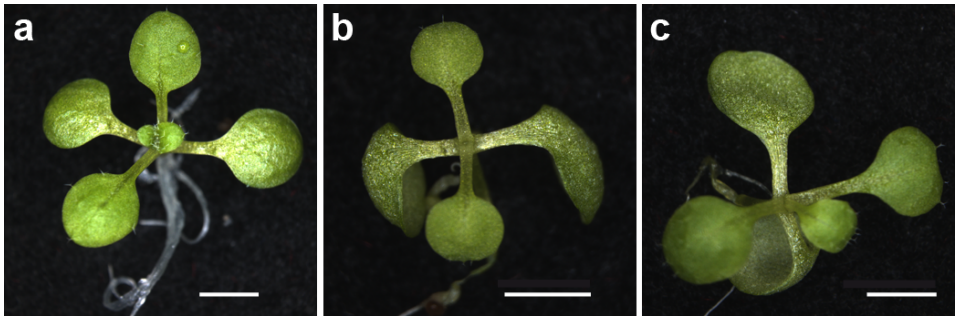

Extended Figure 12: Seedling phenotypes eleven days after germination on auxin supplemented plates.

Phenotypes of seedlings segregating *wus-7* grown on plates containing 10 μm IAA ranged from **a)** unaffected, to **b)** arrested at four leaves stage, or **c)** arrested at five leaves stage with a terminal leaf. Scale bars, 1 mm.

Extended Tables 1-5

	induced			untreated		
	pRPS5a +	*pRPS5a* -	DR5v2 +	*pRPS5a* +	*pRPS5a* -	DR5v2 +
0h	-	-	-	7	0	0
36h	3	**4**	**4**	7	0	0
72h	2	**6**	**6**	7	0	0
120h	2	**3**	**3**	4	0	0

Extended Table 1: Quantification of DR5v2 response after induced stem cell loss.

Plants carrying *DR5v2:3xVENUS-NLS*, *pRPS5a:NLS-tdTomato,* as well as *pCLV3:AlcR/AlcA:CalS3m* were either induced with 1% ethanol or maintained as untreated controls and cohorts were scored for loss of *RPS5a* promoter activity from stem cells and DR5v2 expression by confocal imaging. Stem cell loss and associated DR5v2 activation exclusively occurred in induced plants. All plants with reduced *pRPS5a* activity expressed DR5v2. *pRPS5a* + denotes plants with uncompromised *pRPS5a* promoter activity in stem cells. *pRPS5a* - denotes plants with reduced *pRPS5a* promoter activity in stem cells. DR5v2 + denotes plants with DR5v2 activity in stem cells. Table lists number of individual plants showing reporter expression.

	GO ID	Term	Annotated	Significant	Expected	p-Value
1	GO:0010200	response to chitin	393	145	55.45	2.8E-30
2	GO:0009611	response to wounding	313	109	44.16	1E-20
3	GO:0010363	regulation of plant-type hypersensitive response	336	111	47.41	4.6E-19
4	GO:0006612	protein targeting to membrane	340	111	47.97	1.3E-18
5	GO:0009414	response to water deprivation	374	130	52.77	5.7E-18
6	GO:0009867	jasmonic acid mediated signaling pathway	256	89	36.12	1.2E-15
7	GO:0009733	response to auxin	354	107	49.95	2.3E-15
8	GO:0002679	respiratory burst involved in defense response	114	50	16.09	1.1E-14
9	GO:0009737	response to abscisic acid	548	174	77.32	1.1E-14
10	GO:0009738	abscisic acid-activated signaling pathway	232	78	32.74	1.1E-12
11	GO:0009651	response to salt stress	704	187	99.33	2.6E-12
12	GO:0009695	jasmonic acid biosynthetic process	125	49	17.64	3.4E-12
13	GO:0006857	oligopeptide transport	97	41	13.69	1.1E-11
14	GO:0050832	defense response to fungus	303	84	42.75	3.3E-10
15	GO:0009862	systemic acquired resistance, salicylic acid mediated signaling pathway	222	66	31.32	1.2E-9
16	GO:0042538	hyperosmotic salinity response	152	50	21.45	2.9E-9
17	GO:0009612	response to mechanical stimulus	59	27	8.32	4.5E-9
18	GO:0042742	defense response to bacterium	344	93	48.54	4.9E-9
19	GO:0009684	indoleacetic acid biosynthetic process	94	36	13.26	5.2E-9
20	GO:0006569	tryptophan catabolic process	67	29	9.45	6E-9
21	GO:0009723	response to ethylene	325	101	45.86	1.2E-8
22	GO:0009753	response to jasmonic acid	427	141	60.25	1.2E-8
23	GO:0009873	ethylene-activated signaling pathway	118	41	16.65	1.3E-8
24	GO:0009620	response to fungus	440	132	62.08	2.5E-8
25	GO:0000165	MAPK cascade	197	57	27.8	4.5E-8
26	GO:0009963	positive regulation of flavonoid biosynthetic process	93	34	13.12	5.3E-8
27	GO:0006355	regulation of transcription, DNA-templated	1588	296	224.07	7.1E-8
28	GO:0043069	negative regulation of programmed cell death	158	48	22.29	1E-7
29	GO:0009739	response to gibberellin	143	49	20.18	1.1E-7
30	GO:0031348	negative regulation of defense response	246	65	34.71	2.3E-7
31	GO:0009409	response to cold	539	118	76.05	4.2E-7
32	GO:0009750	response to fructose	127	39	17.92	0.0000011
33	GO:0030968	endoplasmic reticulum unfolded protein response	171	48	24.13	0.0000013
34	GO:0009693	ethylene biosynthetic process	110	35	15.52	0.0000016
35	GO:0009805	coumarin biosynthetic process	51	21	7.2	0.000002
36	GO:0010310	regulation of hydrogen peroxide metabolic process	159	45	22.43	0.0000022
37	GO:0030003	cellular cation homeostasis	146	42	20.6	0.000003
38	GO:0007623	circadian rhythm	156	44	22.01	0.0000032
39	GO:0006833	water transport	118	36	16.65	0.0000034
40	GO:0009741	response to brassinosteroid	102	37	14.39	0.0000036
41	GO:0080167	response to karrikin	114	35	16.09	0.000004

42	GO:0002237	response to molecule of bacterial origin	97	31	13.69	0.0000056
43	GO:0006979	response to oxidative stress	407	90	57.43	0.0000065
44	GO:0006813	potassium ion transport	35	16	4.94	0.0000066
45	GO:0046777	protein autophosphorylation	131	37	18.48	0.000018
46	GO:0006598	polyamine catabolic process	34	15	4.8	0.000022
47	GO:0035556	intracellular signal transduction	446	133	62.93	0.000023
48	GO:0009269	response to desiccation	31	14	4.37	0.00003
49	GO:0031347	regulation of defense response	485	146	68.43	0.00003
50	GO:0009825	multidimensional cell growth	96	29	13.55	0.000037
51	GO:0009697	salicylic acid biosynthetic process	181	46	25.54	0.000037
52	GO:0019344	cysteine biosynthetic process	181	46	25.54	0.000037
53	GO:0006970	response to osmotic stress	749	207	105.68	0.000041
54	GO:0070838	divalent metal ion transport	184	53	25.96	0.000069
55	GO:0009627	systemic acquired resistance	395	109	55.73	0.000077
56	GO:0006949	syncytium formation	19	10	2.68	0.000083
57	GO:0042398	cellular modified amino acid biosynthetic process	50	18	7.06	0.000091
58	GO:0009751	response to salicylic acid	423	122	59.69	0.000098
59	GO:0042631	cellular response to water deprivation	59	20	8.32	0.0001
60	GO:0009965	leaf morphogenesis	186	49	26.24	0.00011
61	GO:0010583	response to cyclopentenone	132	35	18.63	0.00012
62	GO:0001666	response to hypoxia	74	23	10.44	0.00014
63	GO:0007030	Golgi organization	160	40	22.58	0.00017
64	GO:0016126	sterol biosynthetic process	150	38	21.17	0.00018
65	GO:0019748	secondary metabolic process	527	133	74.36	0.00022
66	GO:0006468	protein phosphorylation	620	157	87.48	0.00024
67	GO:0006995	cellular response to nitrogen starvation	21	10	2.96	0.00024
68	GO:0009863	salicylic acid mediated signaling pathway	315	92	44.45	0.00028
69	GO:0009407	toxin catabolic process	180	43	25.4	0.00029
70	GO:0009595	detection of biotic stimulus	92	26	12.98	0.0003
71	GO:0046686	response to cadmium ion	415	84	58.56	0.00033
72	GO:0006816	calcium ion transport	108	29	15.24	0.00036
73	GO:0042335	cuticle development	42	15	5.93	0.00038
74	GO:0009617	response to bacterium	499	140	70.41	0.0004
75	GO:0010264	myo-inositol hexakisphosphate biosynthetic process	51	17	7.2	0.00041
76	GO:0010119	regulation of stomatal movement	47	16	6.63	0.00046
77	GO:0043900	regulation of multi-organism process	115	30	16.23	0.00049
78	GO:0010017	red or far-red light signaling pathway	39	14	5.5	0.00056
79	GO:0010260	animal organ senescence	27	11	3.81	0.00063
80	GO:0009740	gibberellic acid mediated signaling pathway	72	21	10.16	0.0007
81	GO:0007169	transmembrane receptor protein tyrosine kinase signaling pathway	113	29	15.94	0.0008
82	GO:0015824	proline transport	68	20	9.59	0.00083
83	GO:0010227	floral organ abscission	32	12	4.52	0.00088
84	GO:0052541	plant-type cell wall cellulose metabolic process	24	10	3.39	0.0009
85	GO:0010158	abaxial cell fate specification	7	5	0.99	0.00091

86	GO:0009742	brassinosteroid mediated signaling pathway	37	13	5.22	0.0011
87	GO:0048767	root hair elongation	164	38	23.14	0.00117
88	GO:0010118	stomatal movement	86	32	12.13	0.00168
89	GO:0009694	jasmonic acid metabolic process	147	58	20.74	0.00171
90	GO:0033500	carbohydrate homeostasis	12	8	1.69	0.00174
91	GO:0007231	osmosensory signaling pathway	5	4	0.71	0.00175
92	GO:2000022	regulation of jasmonic acid mediated signaling pathway	5	4	0.71	0.00175
93	GO:0010037	response to carbon dioxide	5	4	0.71	0.00175
94	GO:0009624	response to nematode	72	20	10.16	0.0018
95	GO:0006766	vitamin metabolic process	77	21	10.86	0.0018
96	GO:0006865	amino acid transport	228	61	32.17	0.00209
97	GO:0000038	very long-chain fatty acid metabolic process	44	14	6.21	0.00214
98	GO:0046885	regulation of hormone biosynthetic process	8	5	1.13	0.00215
99	GO:0050801	ion homeostasis	205	59	28.93	0.00226
100	GO:0052546	cell wall pectin metabolic process	40	13	5.64	0.00247

Extended Table 2: GO category enrichment analysis of direct WUS targets.

Top 100 enriched categories are shown.

ID	Term	Annotated	Significant	Expected	p-Value
GO:0009733	response to auxin	354	107	49.95	2.3E-15
GO:0090354	regulation of auxin metabolic process	6	4	0.85	0.00467
GO:0010600	regulation of auxin biosynthetic process	5	3	0.71	0.02246
GO:0009926	auxin polar transport	90	20	12.7	0.02424
GO:0060918	auxin transport	93	20	13.12	0.03351

Extended Table 3: Auxin related GO terms enriched among direct WUS targets at $p < 0.05$.

AGI	Gene Name	WUS peaks	Log2FC	p adj.
AT1G59750	ARF1	0	-0.111597744	0.358464723
AT5G62000	ARF2	1	-0.160244055	0.080636193
AT2G33860	ARF3	1	0.74121558	0.000129974
AT5G60450	ARF4	1	-1.260779231	2.78E-12
AT1G19850	ARF5	1	0.824932624	0.00041103
AT1G30330	ARF6	5	0.273665676	0.047298892
AT5G20730	ARF7	0	0.150899027	0.280076124
AT5G37020	ARF8	1	-1.563675792	1.19E-12
AT4G23980	ARF9	1	1.122752639	4.50E-17
AT2G28350	ARF10	2	0.787777365	0.022930942
AT2G46530	ARF11	1	0.895198988	1.60E-07
AT1G34310*	ARF12	0	0	1
AT1G34170*	ARF13	0	0	1
AT1G35540*	ARF14	0	0	1
AT1G35520*	ARF15	0	0	1
AT4G30080	ARF16	0	0.121858649	0.716958625
AT1G77850	ARF17	0	0.820301179	0.002887907
AT3G61830*	ARF18	0	0.959318681	2.10E-08
AT1G19220	ARF19	0	1.078934444	9.14E-09
AT1G35240*	ARF20	0	0	1
AT1G34410*	ARF21	0	0	1
AT1G34390*	ARF22	0	0	1
AT1G43950*	ARF23	0	0	1
AT4G14560	IAA1	1	-0.049017547	0.917632937
AT3G23030	IAA2	2	-0.779787625	9.22E-17
AT1G04240	SHY2	2	3.163647428	9.32E-101
AT5G43700	ATAUX2-11	1	-0.467157239	0.000156676
AT1G15580*	IAA5	0	0	1
AT1G52830	IAA6	2	0.116034132	1
AT3G23050	IAA7	1	0.551262546	9.12E-10
AT2G22670	IAA8	2	1.364381273	4.79E-29
AT5G65670	IAA9	2	0.105183055	0.311631229
AT1G04100*	IAA10	0	-1.683375121	2.55E-12
AT4G28640	IAA11	0	-0.673556893	0.092257616
AT1G04550	IAA12	1	-0.566175948	0.043218198
AT2G33310	IAA13	1	-1.008001464	1.12E-12
AT4G14550	IAA14	2	-0.585607079	0.011992423
AT1G80390	IAA15	0	-0.574441357	1
AT3G04730	IAA16	1	-0.406079449	6.14E-08
AT1G04250	AXR3	1	0.640284515	0.002128125
AT1G51950	IAA18	3	-0.767731853	1.75E-11
AT3G15540	IAA19	2	1.265591239	0.010725483
AT2G46990	IAA20	1	1.864661912	1.06E-15
AT3G16500	PAP1	2	-1.490402367	1.73E-25
AT4G29080	PAP2	1	0.842174986	4.80E-05
AT5G25890	IAA28	0	-0.291255875	0.203663582
AT4G32280	IAA29	0	1.771034915	8.53E-05
AT3G62100	IAA30	0	1.111422364	0.000669299
AT3G17600*	IAA31	0	-0.235206969	1
AT2G01200*	IAA32	0	1.100401196	0.205623963
AT1G15050*	IAA34	0	-0.423041078	0.426177309
AT4G03190	AFB1	0	-1.525054649	4.66E-10
AT3G26810	AFB2	2	-0.162976188	0.363114532
AT1G12820	AFB3	0	1.171943219	5.46E-33
AT4G24390	AFB4	0	0.554308915	0.003823998
AT5G49980	AFB5	1	0.454882856	0.000299204
AT3G62980	TIR1	1	-0.886064319	4.74E-14
AT1G73590	PIN1	1	0.097477956	0.872138329
AT5G57090	PIN2	0	0.609007336	0.190482509
AT1G70940	PIN3	2	-1.183821577	5.24E-22
AT2G01420	PIN4	3	0.34302747	0.001748035
AT5G16530*	PIN5	0	-0.181089018	1
AT1G77110	PIN6	1	1.037619295	0.205625501
AT1G23080	PIN7	2	-0.188145814	0.217710653
AT5G15100	PIN8	0	0	1
AT2G38120	AUX1	2	0.877290156	2.64E-09
AT5G01240	LAX1	2	0.138928766	0.245947254
AT2G21050	LAX2	0	0.415613371	0.277081161
AT1G77690	LAX3	1	-0.008043826	0.977318196
AT2G34650	PID	2	0.319524941	0.197369125
AT2G26700	PID2	0	-0.126731923	0.818644213

Extended Table 4: Response of auxin signalling to WUS.

Adjusted p-value for RNA-seq data was calculated using the Benjamini-Hochberg method in Deseq2 (ref. 46). Asterisks denote genes in regions with closed chromatin[19].

AGI	Name	Responsive to auxin	Expression PZ>CZ	Promoter bound by WUS	Responsive to WUS
AT3G62980	*TIR1*	x	x	x	x
AT2G33860	*ARF3*	x	x	x	x
AT5G60450	*ARF4*	x	x	x	x
AT1G19850	*ARF5 (MP)*	x	x	x	x
AT2G22670	*IAA8*	x	x	-	x
AT5G65670	*IAA9*	x	x	x	x
AT1G04550	*IAA12 (BDL)*	x	x	-	-
AT5G60200	*TMO6*	x	x	x	x
AT1G74500	*TMO7*	x	-	-	-
AT3G25710	*TMO5*	x	-	-	x
AT4G23750	*TMO3*	x	-	x	x
AT1G68510	*LBD42*	-	-	x	-
AT3G49940	*LBD38*	-	-	x	x
AT3G58190	*LBD29*	x	-	-	-
AT3G11280		x	x	x	x
AT3G28910	*MYB30*	x	x	x	x
AT5G58900		x	x	x	-

Extended Table 5: WUS targets functionally tested by expression from *pCLV3* promoter.

Expression domains in the SAM are based on refs. [12,36,37].

Purpose	Gene	Name	Sequence
genotyping	*wus-7*	A05337	CCGACCAAGAAAGCGGCAACA
		A05338	AGACGTTCTTGCCCTGAATCTTT
Cloning	*MP*	A04634	aacaGGTCTCaggctcaacaATGATGGCTTCATTGTCTTGTGTTG
		A04635	aacaGGTCTCtAGACCCGCATATCGCCTTACGGTA
		A04636	aacaGGTCTCGGTCTaAGCTCTCAGTTGGTATGAGATTTG
		A04637	aacaGGTCTCtAGACCGTTCAACTGAGTGTCCCAC
		A04638	aacaGGTCTCGGTCTaAAGTTTGACCAGTTCAGTCCCTTG
	At4g24550 terminator	72A4	ACTAGGATCCTGTTTTCAGATAATGTTTATCCTTC
		72A5	ACTACTCGAGATCGTTGCACCTTTATTTC
	MPΔ	A04640	aacaGGTCTCtctgaGGTTCGGACGCGGGGTGTCGCAATT
		A04634	aacaGGTCTCaggctcaacaATGATGGCTTCATTGTCTTGTGTTG
	TIR1	A04641	aacaGGTCTCaggctcaacaATGCAGAAGCGAATAGCCTTGTCGT
		A04642	aacaGGTCTCtAGACCATCGGTGGAGAAGCCTTCG
		A04643	aacaGGTCTCGGTCTaGCTGCTATCGCTGCCACTTGCAGG
		A04644	aacaGGTCTCcCTCGAGTCCGGTGCACCCCGTTCA
		A04645	aacaGGTCTCCCGAGgCCAGAGAGCTGCCCTGTTGAGAGA
		A04646	aacaGGTCTCtctgaTAATCCGTTAGTAGTAATGATT
	AT5G58900	A05617	aacaGGTCTCaggctcaacaATGGAGGTTATGAGACCGTCGACGT
		A05618	aacaGGTCTCtctgaTAGTTGAAACATTGTGTTTTGGGCG
	LBD29	A05621	aacaGGTCTCaggctcaacaATGACTAGTTCCAGCTCTAGCTCTG
		A05622	aacaGGTCTCtctgaCGAGAAGGAGATGTAGCCAAAATTT
	LBD38	A05623	aacaGGTCTCaggctcaacaATGAGTTGCAATGGTTGTCGAGTTC
		A05624	aacaGGTCTCtctgaAGCGAAGAGATTGAGCAACTTTGTC
	LBD42	A05625	aacaGGTCTCaggctcaacaATGAGAATCAGCTGCAACGGGTGTA
		A05626	aacaGGTCTCtctgaACCAAGTCTGAGCTCTAAGCCAACC
	MYB30	A05627	aacaGGTCTCaggctcaacaATGGTGAGGCCTCCTTGTTGTGACA
		A05628	aacaGGTCTCtctgaGAAGAAATTAGTGTTTTCATCCAAT
	TMO3	A05629	aacaGGTCTCaggctcaacaATGGAAGCGGAGAAGAAAATGGTTC
		A05630	aacaGGTCTCtctgaAACAGCTAAAAGAGGATCCGACCCG
	TMO5	A05631	aacaGGTCTCaggctcaacaATGTACGCAATGAAAGAAGAAGACT
		A05632	aacaGGTCTCtctgaATTATAACATCGATTCACCATCTTA
	TMO6	A05633	aacaGGTCTCaggctcaacaATGGATCATTTGTTACAACACCAGG
		A05634	aacaGGTCTCtctgaCATTAAAGCACCAGAATTAATGTAG
	TMO7	A05635	aacaGGTCTCaggctcaacaATGTCGGGAAGAAGATCACGTTCGA
		A05636	aacaGGTCTCtctgaTTGGGTAAGTAAGCTTCTGATTAAA
	AT3G11280	A05637	aacaGGTCTCaggctcaacaATGGAGACTCTGCATCCATTCTCTC
		A05638	aacaGGTCTCtctgaAGCTCCGGCACTGAAGACATTTTCT
	ARF3	A06245	gaacaGGTCTCaggctcaacaATGGGTGGTTTAATCGATCT
		A06246	gaacaGGTCTCtctgaGAGAGCAATGTCTAGCAACA
	ARF4	A06823	aacaGGTCTCaggctcaacaATGGAATTTGACTTGAATACTGAG
		A06824	aacaGGTCTCtctgaAACCCTAGTGATTGTAGGAGA
	IAA8	A06825	aacaGGTCTCaggctcaacaATGAGTTCTGGGAACGATAAG
		A06826	aacaGGTCTCtctgaAACCCGCTCTTTGTTCTTCG
	IAA9	A06827	aacaGGTCTCaggctcaacaATGTCCCCGGAAGAGGAGC
		A06828	aacaGGTCTCtctgaAGCTCTCATCTTCGATTTCTCCATT
	IAA12 (BDL)	A04647	aacaGGTCTCaggctcaacaATGCGTGGTGTGTCAGAATTGGAGG
		A04650	aacaGGTCTCtctgaAACAGGGTTGTTTCTTTGTCTATCC

Extended Table 6: Oligonucleotides used in this study

METHODS

Plant material and treatments

All plants were grown at 23 °C in long days or continuous light. Ethanol inductions were performed by watering with 1% ethanol and continuous exposure to ethanol vapour, refreshed every 12 hours. WUS-GR was induced by submerging seedlings in 25 µM dexamethasone, 0.015% Silwet L-70 in 0.5x MS for 2 hours. For local induction at the SAM, 10 *µ*l induction solution were directly applied to the primary inflorescence meristem. Auxin plates were 0.5x MS, 1% agar, pH 5.7, 10 *µ*m IAA. For TSA/IAA cotreatments, shoot apical meristems were dissected from about 4 cm high stem and cultured *in vitro* in Apex Growth Medium (AGM) overnight[38]. AGM was supplemented with vitamins (Duchefa M0409), cytokinin (200 nM 6-Benzylaminopurine), and IAA (3-indole acetic acid, 1 mM) and/or Trichostatin A (TSA, Sigma, T8552, final concentration 5 *µ*M) or mock before pouring. IAA stock solution (0.1 M in 0.2 M KOH) was diluted with 2 mM M.E.S (pH 5.8) to 1 mM working solution, then added to the plates for 30 min before imaging on the second day.

For WUS-induction with TSA treatments, seedlings were submerged in DEX (10 *µ*M) or TSA (1 *µ*M) solution or both, slowly shaken for 2 h, and then harvested for RNA-seq.

All plants were of Col-0 accession apart from *wus-7*, which was in L*er* background. For experiments involving *wus-7*, L*er* plants were used as controls.

Transgenes

The *R2D2* and *pDR5v2:3xVENUS-NLS* lines have been described in ref. 11. *pDR5v2:tdTomato-Linker-NLS:trbcS* was transformed into heterozygous *wus-7* plants and L*er* control plants and activity patterns were scored in T1. A stable single insertion T3 line of *pDR5v2:ER-EYFP-HDEL:tAt4g24550* was used for transformation with *pCLV3:3xmCherry-NLS* and signals were scored in T1. For deGradFP the anti-GFP nanobody coding sequence (*NSlmb-vhhGFP4)*[18] was brought under control of the AlcR/AlcA system[39] and transformed into a stable *pWUS:WUS-linker-GFP wus* rescue line (GD44, described in ref. 4) or an *pUBI10:GFP-NLS* line as control. Experiments were performed in stable single insertion T3 lines. Similarly, the *pCLV3:AlcR/AlcA:CalS3m* line[4] was crossed to *pDR5v2:3xVENUS-NLS, pRPS5a:NLS-tdTomato* and F3 single insertion progeny was used for experiments. For ectopic WUS induction lines *mCherry* was fused N-terminally to the ligand-binding domain of the rat glucocorticoid receptor (GR) and linked by (AAASAIAS[SG]11SAAA)

to the *WUS* coding sequence under control of the *pUBI10* promoter. A single insertion homozygous line was used for crossings, in RNA-seq, and ChIP-seq.

The *pHMG* promoter corresponds to 1347 bp upstream of the AT1g76110 locus. Most constructs were assembled using GreenGate cloning[40]. All oligonucleotides are listed (Extended Table 5).

Microscopy

Confocal microscopy was carried out on a Nikon A1 Confocal with a CFI Apo LWD 25× water immersion objective (Nikon Instruments) as described[4]. 1 mg/ml DAPI was used for cell wall staining.

Image analysis

Quantitative image analysis was done on isotropic image stacks using Fiji (v1.50b)[41], MorphoGraphX[42], ilastik[43], Matlab (Release 2014b, The MathWorks, Inc., United States) and KNIME[44]. Signal quantification methods: all images for an experimental set were captured under identical microscope settings and signal intensities were never adjusted, making intra-experiment signal comparisons possible. MorphographX analysis was performed according to standards defined in the user manual. Averaging and statistical analysis of signals across meristems was performed as follows: histograms of signal intensities along 100 central cross-sections per SAM were (cross-sections rotated by 3.6 degrees successively) were measured by ImageJ standard function. Signals were centered for comparison between individuals. Signals +/- 12.5μm around the SAM center were compared between treatment and control and tested for significance by Student's T-test. Distance from center with signal up to 120% of center background signal between treatment and control was determined and tested by Student's T-test.

To determine the center of an inflorescence meristem, 10 to 20 L1 cells located at the meristem summit were segmented using the carving workflow in ilastik. A sphere was fitted through the centroids of these cells using the least squared distances method. The sphere was superimposed on the original DAPI stained image volume to help identifying the newly emerging flower primordia. Three points marking the center of three young flower primordia were manually picked close to the sphere surface, projected onto the sphere and then used as seeds to perform a spheric voronoi tessellation (https://de.mathworks.com/matlabcentral/fileexchange/40989-voronoi-sphere). The point P_{center} is equidistant to the three seed points and serves as a good approximation for the meristem center which is marked by the *pCLV3* stem cell reporter. The method was tested using image stacks of nine meristems containing cell

walls stained by DAPI in one channel and the stem cell marker *pCLV3::mCherry-NLS* in the second channel. The computationally estimated meristem center and the one determined by *pCLV3:mCherry-NLS* expression in every case were in the range of one cell diameter. Further details and workflows are available on request.

In situ hybridization

In-situ hybridizations were carried out as described[45] .

ChIP-seq and RNA-seq

All experiments were carried out on 5 day old seedlings grown on 0.5 MS plates after 2 hours of either Dex or mock treatment. ChIP assays were performed from 3g of fresh weight each as described in ref. 46 using RFP-Trap single chain antibodies (Chromotek). Enrichment of specific DNA fragments was validated by qPCR at the *ARR7* promoter region[24]. Two independent libraries were generated for the *WUS-GR* and control ChIP each using pooled DNA from 6 to 9 individual ChIP preparations. RNA-seq was carried out in biological triplicates. After careful benchmarking of our WUS-GR line, we find it to be the most potent and consistent tool for WUS induction to date, affording a much higher sensitivity for identifying transcriptional targets. In addition, the use of RFP-trap increased sensitivity of the ChIP assay. Consistently, we were able to identify 5874 genomic regions bound by WUS in both ChIP-seq experiments at $p < 0.05$, which corresponded to 4515 genes. This compared to 136 regions we had previously identified by ChIP-chip[20], highlighting the increase in power. Previously identified direct targets, such as *ARR7, CLV1, KAN1, KAN2 AS2* and *YAB3*[20,21,24] were also picked up in our analysis. Because of the medium level ubiquitous expression of WUS, both RNA-seq and ChIP-seq capture the global regulatory potential of WUS. Since regulatory output of WUS is dependent on tissue context, targets identified here might not be relevant for all tissues. In addition, targets might be induced by WUS in one tissue and repressed in another, which cannot be resolved by this dataset. All genomic datasets are available under GEO accession: GSE97065

Bioinformatics

ChIP-seq data were mapped to TAIR10 genome by BWA aligner (v0.7.17) [47] on a local Galaxy instance (v17.09)[48]. Peak calling was performed using Hiddendomains (v3.0)[49]. Peaks were annotated to TAIR10 genes using PAVIS[50] .

Alignment of RNA-seq reads to TAIR10 genome by HISAT2 (v2.1.0)[51] and calculation of count matrices by featureCounts (v1.6.3)[52] was done on Galaxy instance. Differentially expressed genes were identified with R bioconductor package Deseq2 (1.20.0)[53]. Gene ontology analysis was carried out using topGO R package (v2.32.0) with all genes annotated to open chromatin[19] as background.